

## LASER EQUIPPED ION STORAGE AND COOLER RING, S-LSR

A. Noda\*, H. Fadil, S. Fujimoto, M. Ikegami, Y. Iwashita, S. Nakamura, T. Shirai,  
 M. Tanabe, H. Tongu, ICR, Kyoto University, Uji-city, Kyoto Japan  
 K. Matsukado, K. Noda, S. Shibuya, T. Takeuchi, S. Yamada, NIRS, Chiba, Japan  
 H. Daido, Y. Kato, T. Tajima, APRC, JAERI KANSAI, Kizu, Kyoto, Japan  
 M. Beutelspacher, M. Grieser, MPI, Heidelberg, Germany  
 E. Syresin, JINR, Dubna, Russia

### Abstract

Ion storage and cooler ring, S-LSR, with the average radius and maximum magnetic rigidity of 3.59 m and 1.0 Tm, respectively is now under construction. Major research scopes at S-LSR are collection and electron-cooling of laser-produced ion beam and approach to ultra cold ion beam with use of the laser cooling. Start of the beam commissioning is scheduled from the spring 2005.

### INTRODUCTION

Recently cancer therapy with use of charged particle has realized very promising clinical results and especially, the carbon beam has attained prominent results due to its high radio biological effectiveness (RBE) [1]. The size of the facility and its construction and operation costs, however, have been rather large compared with the photon treatment facility, which has been a bottle neck for widespread use of such a treatment. For the purpose of downsizing of cancer therapy facility with use of charged particles, possibility of utilizing very high electromagnetic field created by a high power laser has been studied [2]. Production of ions with the energy of several tens MeV by high power lasers has been reported [3,4]. Their intensities, however, decrease exponentially and have no peak in the energy spectrum. In the present scheme, carbon beam with kinetic energy of 2 MeV/u  $\pm$  5% is to be selected and then phase rotated with use of an RF electric field which is synchronized to the pulse laser in phase. The energy spread of  $\pm$ 1% after phase rotation is to be cooled down another one order of magnitude after injection into S-LSR by an electron cooling.

On the other hand, approach to ultra cold state of the circulating beam has collected strong concerns from the point of view of beam physics since the report about ordering from the group at NAP-M in 1984 [5]. Recently, similar experimental results indicating one dimensional ordering are reported from GSI and Manne Siegbahn Laboratoty [6, 7]. Three dimensional beam crystallization at circular trap is also reported for very low energy beam (<1 eV), which is

reported to collapse suddenly by acceleration to higher energy [8], which seems due to shear force caused by deflection. In order to avoid this situation, necessity of tapered cooling is claimed [9], which, however, has not yet been realized up to now. As the approach to improve this situation, we are investigating the possibility to suppress the shear force by overlapping the radial electric field in the dipole magnetic field [10].

From the above mentioned scientific motive force, S-LSR is now under construction at ICR, Kyoto University by collaboration with NIRS in the building next to the high-power (10 TW) short-pulse (~100fs) laser (T6 laser) as shown in Fig. 1. The main magnets of S-LSR have already been completed and their evaluation is now under way. A compact electron cooler is almost completed and its evaluation through field measurements is just to be started.

In the present paper, the S-LSR project is described at first and then its present status of construction is presented.

### COLLECTION AND PHASE ROTATION OF LASER-PRODUCED IONS

In recent years, plasmas produced by the intense laser open up the new type of hard X-ray, neutrons, electrons and high-energy ion sources. So as to develop laser ion source as an injector of a compact ion-synchrotron for cancer therapy, ion production by irradiation of a high-

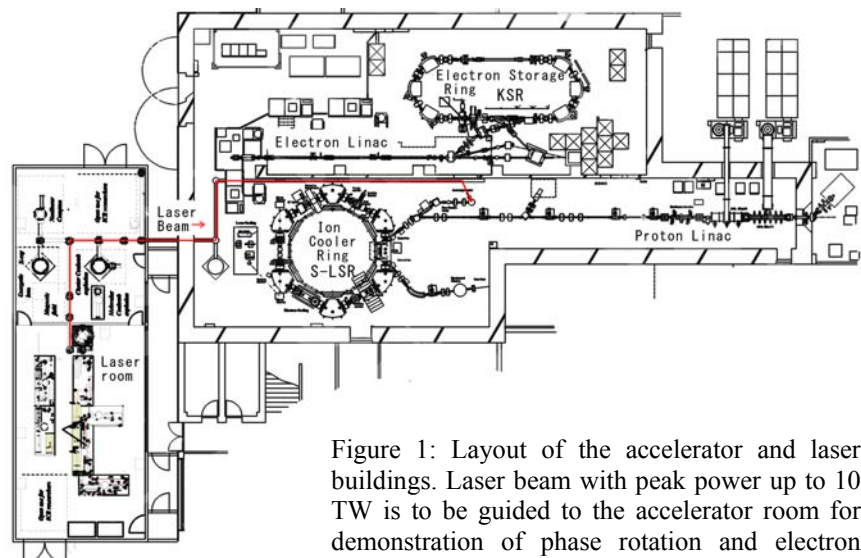


Figure 1: Layout of the accelerator and laser buildings. Laser beam with peak power up to 10 TW is to be guided to the accelerator room for demonstration of phase rotation and electron cooling of laser-produced ion beam.

\*noda@kyticr.kuicr.kyoto-u.ac.jp

power (100 TW) short-pulse (20 fs) laser with high repetition rate (10 Hz) at JAERI, Kansai has been prepared and the first experiment is scheduled in the summer of 2004. The RF cavity installed at the downstream of the target chamber of 100 TW laser is shown in Fig. 2. Preparatory experiments have been performed with use of 3 TW 50 fs laser operated by 1 Hz focused on Ta foils, 5 μm in thickness. Produced ion beam was detected with use of a Thomson parabola as shown in Fig. 3. The experimental data showed the fact that the ion production can be explained by the production from under dense plasma for such



Figure 2: RF cavity for phase rotation installed after the target chamber of 100 TW laser.

Produced ion beam was detected with use of a Thomson parabola as shown in Fig. 3. The experimental data showed the fact that the ion production can be explained by the production from under dense plasma for such

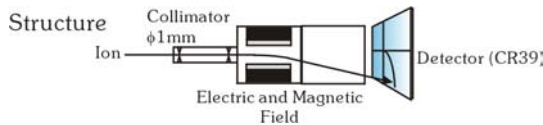


Figure 3: Thomson parabola used for detection of laser produced ion beam.

a case with presence of pre-pulse as the present case [11] (see Fig. 4). The laser produced ion has no energy peak but decreases in its intensity according to increase of its energy as shown in Fig.4.

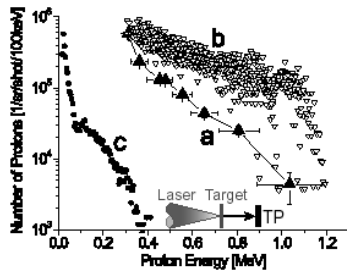


Figure 4: Energy spectrum of laser produced ions .a: experimental results from Ta 5μm foil, b: simulation assuming under dense plasma and c: simulation with over-dense plasma. (Ref. [11])

This situation is to be modified by phase rotation utilizing an RF electric field synchronized to the pulse laser.

### ELECTRON COOLING

The phase rotated ion with the energy spread of ±1% is further cooled down by an electron beam cooling so as to be able to be accelerated by a pulse synchrotron the the higher energy (several hundreds MeV) needed for cancer therapy. For this purpose, sweeping the relative velocity between the ion beam and the electron is proposed and proof of principle experiments have been performed at TSR of Max-Planck-Institut für Kernphysik in Germany [12]. The cooling rate, however, depends on the transverse emittance of the ion beam and it is inevitable to apply such an electron cooling for real laser produced ions. For this purpose, a compact electron cooler for S-LSR is now under construction. It has been designed and

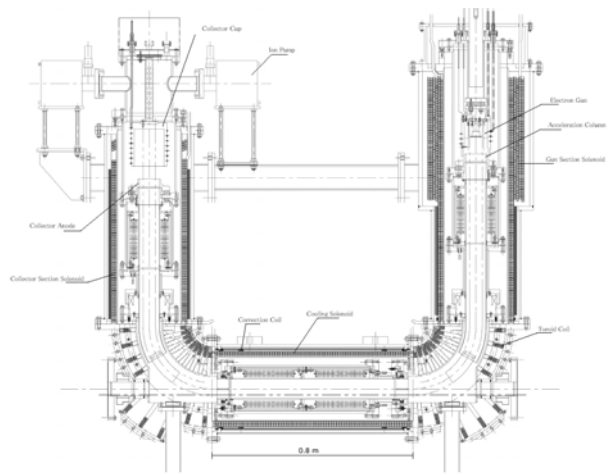


Figure 5: Schematic layout of the S-LSR electron cooler. optimized for operation in two modes corresponding to 2 MeV/u carbon beam and 7 MeV proton beam. The main parameters of the electron cooler are summarized in table 1, and Fig. 5 shows the schematic layout of the device. The limited space in the straight section of the S-LSR ring puts stringent restrictions on the length of the cooling section and the radius of the equilibrium electron orbit inside the toroidal sections, which are 0.8 m and 0.25 m respectively. The maximum magnetic field in the gun section is 1.5 kG, and in the cooling section 0.5 kG. The adiabatic expansion of the electron beam achieves a reduction of the transverse temperature by a factor 3 compared with the case without such an expansion. The magnetic field in the cooling section was optimized utilizing 3-dimensional calculations, and a good field region length of about 50 cm is achieved with the transverse field better than

$$\frac{B_{\perp}}{B_0} \leq 5 \cdot 10^{-4}$$

where  $B_0=500$  G is the longitudinal field.

The electron gun consists of a flat cathode of diameter 30mm, a Pierce electrode and an extraction anode of aperture 60 mm. The calculated Perveance is 2.2 μP. For cooling of the carbon beam, the maximum electron current is 80 mA and more than 400 mA is applied for cooling of proton beam.

Table 1 Parameters of the S-LSR electron cooler

Cooler solenoid length	0.8 m
Bending toroid radius	0.25 m
Magnetic field (gun/cooling)	1.5/0.5 kG
Maximum adiabatic expansion factor	3
Field uniformity in cooling solenoid	$5 \times 10^{-4}$
Electron energy	1 - 5 keV
Cathode radius, mm	15
Electron beam current	0.05 - 0.4 A
Gun Perveance	2.2 μP
β-function at cooling section	1.7/2.4 m

**PRESENT STATUS OF S-LSR**

*Lattice Structure*

The lattice of S-LSR has six-fold symmetry in order to enable the crystalline mode where betatron phase advance per period is less than 90° both in horizontal and vertical directions. Main parameters of S-LSR are listed up in Table 2. So as to suppress the shear force in dipole section, the radial electric field is overlapped with the dipole magnetic field as shown in Fig. 6. Detailed design of the electrode is described later.

Table 2 Major parameters of S-LSR

Ring	
Circumference	22.557 m
Average radius	3.59 m
Length of straight section	2.66 m
Number of periods	6
Betatron Tune	
Crystalline Mode	1.45 (H) , 1.44 (V)
Normal Operation Mode	1.872(H), 0.788 (V)
Bending Magnet (H-type)	
Maximum field	0.95 T
Curvature radius	1.05 m
Gap height	70 mm
Pole end cut	Rogowski cut+Field clamp
Deflection Angle	60°
Weight	4.5 tons
Quadrupole Magnet	
Core Length	0.20 m
Bore radius	70 mm
Maximum field gradient	5 T/m

*Dipole Magnet*

Dipole magnets of S-LSR are made by H-type with the cross section shown in Fig. 7. Design of the magnets has been fixed by using 2D and 3D magnetic-field calculation codes POISSON and TOSCA. The magnets have a gap of 70 mm and the pole width of 371 mm as seen in Fig. 7 [13]. Their field properties are evaluated with use of Hall probes precisely position controlled with use of pulse motors and ball screws. The measured field uniformity is better than a few times 10<sup>-4</sup> in the enough inner region of

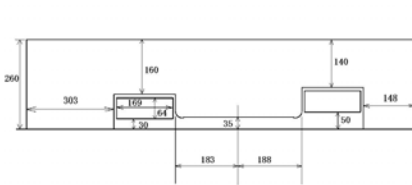


Figure 7: Cross-section of the dipole magnet. The gap height and pole width are 70 mm and 371 mm, respectively

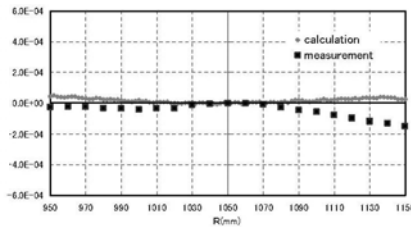


Figure 8: Field uniformity of the dipole magnet in radial direction ±100 mm from the reference orbit.

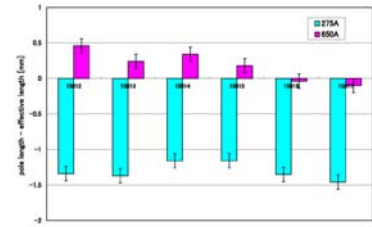


Figure 9: The differences of effective lengths and pole lengths of the 6 dipole magnets.

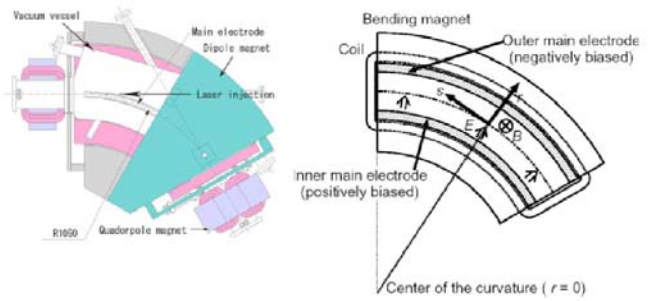


Figure. 6: Electrodes installed inside the dipole magnet.

the gap as shown in Fig. 8. The effective length is also evaluated integrating the field mapped data assuming the field flatness well inside the gap. Deviations of the effective length among the 6 dipole magnets are shown in Fig. 9 for excitation currents of 275 A and 650 A corresponding the field levels of 4.34 kG and 9.85 kG, respectively. As is known from the figure, the variation of the effective length is less than ±2.5×10<sup>-4</sup>

*Quadrupole Magnet*

The quadrupole magnet for S-LSR has core length and bore radius of 0.2 m and 70 mm, respectively. Its distance from the dipole magnet is only 200 mm, where field clamp of the dipole exists as shown in Fig. 10. Design study of quadrupole magnets for S-LSR was performed taking into account of the effect by the presence of a field clamp of an adjacent bending magnet. The design optimisation was carried out by using the 3D magnet-static field calculation code, TOSCA [14]. Optimised results for the conditions without and with the field clamp are shown in Fig. 11(a) and (b), respectively. Corresponding measured data are given in Fig. 12. It is known from these figures that evaluation of the field property of the quadrupole magnet together with the presence of the field clamp of the dipole magnet is inevitable. Precise evaluation of the quadrupole magnets with use of a translation coil has just been started.

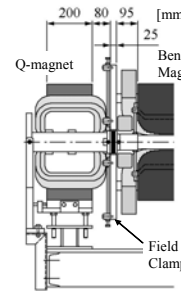


Figure 10: Side view of the quadrupole magnet adjacent to the dipole magnet of S-LSR

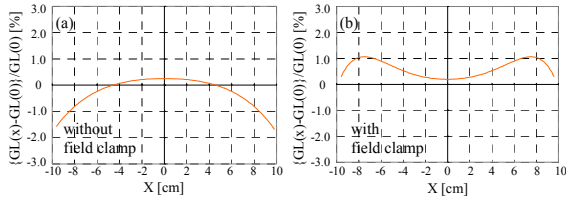


Figure 11: The horizontal distribution of the integrated field gradient error in the cases without (a) and with (b) field clamp effect.

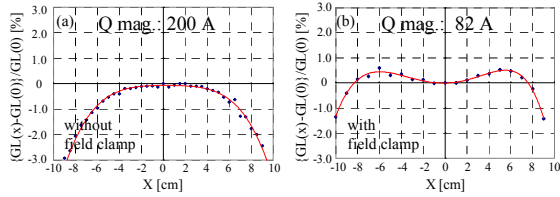


Figure 12: Measured horizontal distribution of the integrated field gradient error for the conditions without (a) and with (b) the presence of the field clamp of the dipole magnet.

**Vacuum System**

Evacuation system of S-LSR consists of 2 NEG pumps (200 l/sec) installed into each chamber inside the dipole magnet and NEG pumps installed into the electron cooler (430l/sec, 330 l/sec) and ion pumps set at straight sections as shown in Fig. 13. The attained vacuum pressure is estimated as shown in Fig. 14 assuming the pre-baking in vacuum during 2 hours at 950°C so as to reduce the out-gassing rate. It is known from the figure that the average pressure of  $5 \times 10^{-9}$  Pa will be attained after long term aging. For this condition, the beam life time of  $^{24}\text{Mg}^+$  with the kinetic energy of 35 keV, which is considered to be shortest, is estimated to be 8 sec.

**Beam Monitore**

Two types of beam monitors have been developed for S-LSR. One is a non-destructive beam profile monitor utilizing Micro-Channel Plate (MCP). The beam ionizes the residual gases. Ions created in such ionization process

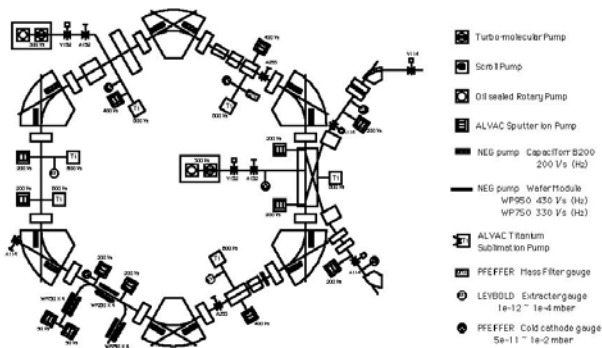


Figure 13: Evacuation system of S-LSR

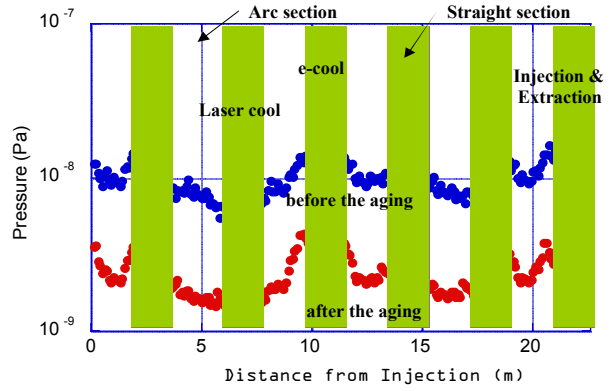


Figure 14: Estimated equilibrium vacuum pressure at S-LSR.

are projected by the uniform electric field and then detected by a position sensitive detector (MCP).as shown in Fig. 15 (a). In Fig. 15 (b), the fabricated beam profile monitor is shown. Typical spatial resolution of this type of monitor is estimated to be ~0.3 mm..

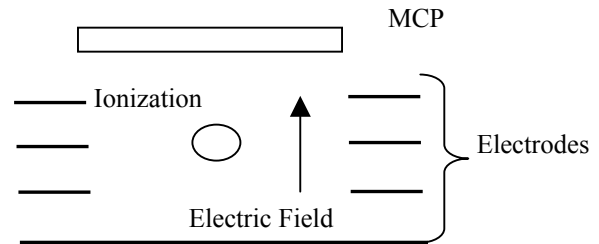


Figure 15(a): MCP Beam Profile Monitor.

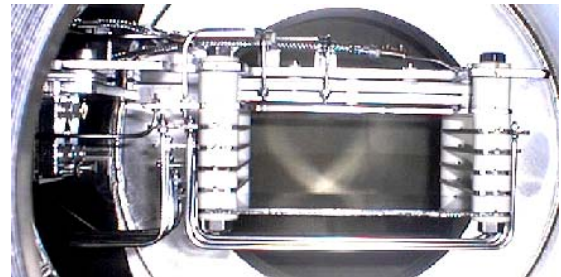


Figure 15(b): Photograph of the fabricated Beam Profile Monitor.

The other monitor detects the induced charges on electrodes by circulating beam (Electro Static Pick Up). Due to very tight geometrical constraint of S-LSR, such electrodes are decided to be installed into the chamber inside the quadrupole magnet as shown in Fig. 16. This monitor is set at all the quadrupole magnets of S-LSR, 12 in total and will be utilized for correction of the closed orbit distortion.

**APPROACH TO ULTRA-COLD STATE**

In order to control the dispersion, the radial electric field is to be superposed with the dipole magnetic field as is mentioned already. The electrodes, however, must be installed in a rather limited aperture inside the vacuum chamber in the gap of dipole magnet, 70 mm in height. It is anticipated that the uniformity of the electric field is not

so good due to limited height of the electrodes compared with the distance of 30 mm between the electrodes. So as to realize a good quality of electric field, usage of intermediate electrodes is proposed as shown in Fig. 17. Good uniformity in a limited region around the central orbit is realized by adjusting the potential of each intermediate electrode as shown in Fig. 18. The electrodes system above mentioned can be moved away to the sheltering position at the inner side for normal operation without such radial electric field so as to keep enough aperture of  $\pm 100$  mm.

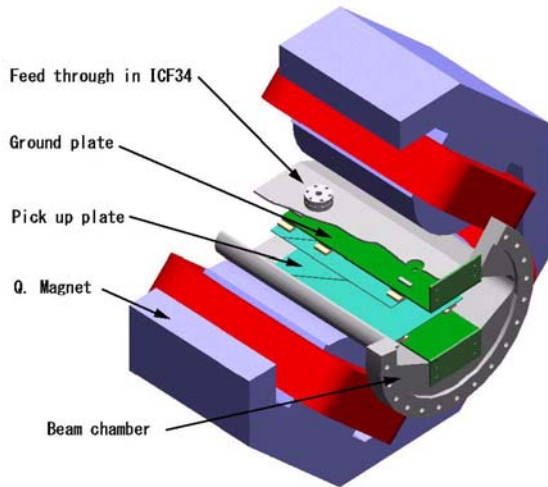


Figure 16: Beam position monitor to be set in the chamber inside a quadrupole magnet.

By application of a radial electric field superposed with the dipole magnetic field, the ion beam circulating the outer orbit than the central one will be accelerated at the entrance of the dipole section and will be decelerated at the exit from the dipole. For ion beam circulating the inner orbit, the opposite situation will take place. Such

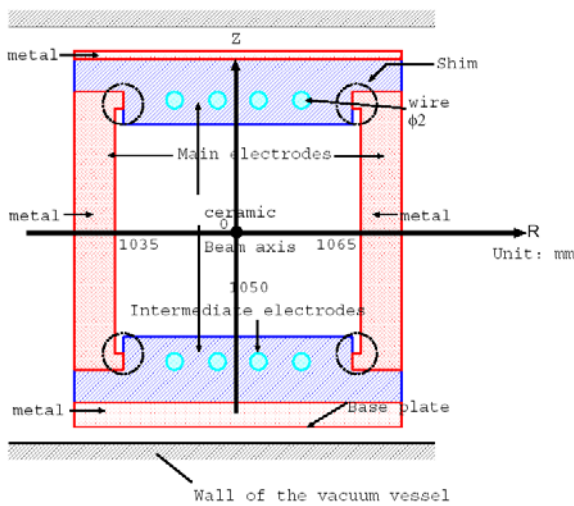


Figure 17: Cross sectional View of the electrodes installed into the chamber inside the dipole magnet.

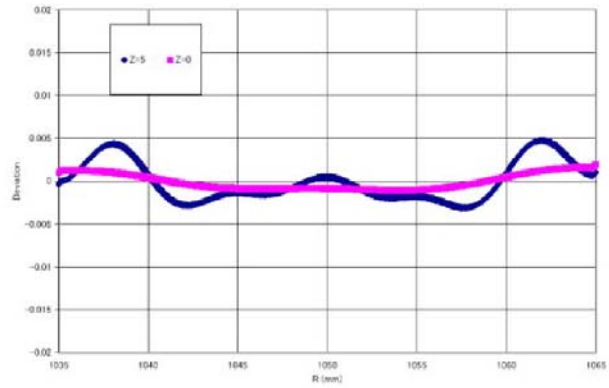


Figure 18: Field uniformity realized by the use of the intermediate electrodes. Deviations at  $z=0$  mm (median plane) and  $z=5$  mm are shown.

situation is expected to reduce the effect of shear force at the dipole section because the angular velocity is expected to be kept the same even with difference of the orbit length by such velocity difference attained with the electrostatic potential difference [15], which is to be experimentally tested at S-LSR although further quantitative analytical investigation is needed in parallel..

## ACKNOWLEDGEMENTS

The work presented here has been financially supported by the Advanced Compact Accelerator Development Project by Ministry of Education, Culture, Sports, Science and Technology.

## REFERENCES

- [1] S. Yamada, Proc. 2<sup>nd</sup> APAC, Beijing (2001) pp829-833.
- [2] A. Noda et al., Proc. EPAC 2002, Paris, pp2748-2750.
- [3] P. Stephen et al., Physics of Plasma 7 (2000) pp2076-2082.
- [4] E.L. Clark et al., Phys. Rev. Lett. 85 (2000) pp1654-1657.
- [5] V.V. Parkhomchuk, Proc. ECOOL 1984, Karlsruhe (1984), p71.
- [6] M. Steck et al., Hyperf. Int. 99 (1996), p245.  
M. Steck et al., Phys. Rev. Lett. 77 (1996), p3803.
- [7] H. Danared et al., Phys. Rev. Lett. 88 (2002) 174801.
- [8] U. Schlam et al., J. Phys. B36 (2003) PP561-
- [9] H. Okamoto and J. Wei, Phys. Rev. E58 (1998) pp3817-3825.
- [10] M. Ikegami et al., Submitted to Phys. Rev. ST-AB.
- [11] K. Matsukado et al., Phys. Rev. Lett. 91 (2003) 215001.
- [12] H. Fadil et al., Nucl. Instr. Meth. A517 (2004), pp1-8.
- [13] M. Ikegami et al., Beam Science and Technology, 8 (2003). Pp5-8.
- [14] T. Takeuchi et al., Beam Science and Technology, 8 (2003), pp. 13-18.
- [15] H. Okamoto, private communication.